

The Total Energy Flux Leaving the Ocean's Mixed Layer

ANTONIJA RIMAC^a AND JIN-SONG VON STORCH

Max Planck Institute for Meteorology, Hamburg, Germany

CARSTEN EDEN

Institut für Meereskunde, Universität Hamburg, Hamburg, Germany

(Manuscript received 23 June 2015, in final form 4 March 2016)

ABSTRACT

The total energy flux leaving the ocean's spatially and seasonally varying mixed layer is estimated using a global $1/10^\circ$ ocean general circulation model. From the total wind-power input of 3.33 TW into near-inertial waves (0.35 TW), subinertial fluctuations (0.87 TW), and the time-mean circulation (2.11 TW), 0.92 TW leave the mixed layer, with 0.04 TW (11.4%) due to near-inertial motions, 0.07 TW (8.04%) due to subinertial fluctuations, and 0.81 TW (38.4%) due to time-mean motions. Of the 0.81 TW from the time-mean motions, 0.5 TW result from the projection of the horizontal flux onto the sloped bottom of the mixed layer. This projection is negligible for the transient fluxes. The spatial structure of the vertical flux is determined principally by the wind stress curl. The mean and subinertial fluxes leaving the mixed layer are approximately 40%–50% smaller than the respective fluxes across the Ekman layer according to the method proposed by Stern. The fraction related to transient fluctuations tends to decrease with increasing depth of the mixed layer and with increasing strength of wind stress variability.

1. Introduction

Interior density mixing contributes to drive the large-scale ocean circulation. The energy needed for this mixing is believed to be supplied predominantly by the tidal and wind forcing (Munk and Wunsch 1998). In this study, we focus on the wind-power input to three different types of motions, that is, *near-inertial motions*, *subinertial fluctuations*, and *time-mean flows*. Surface winds can generate near-inertial waves that propagate freely into the ocean's interior and after escaping the mixed layer contribute to interior mixing (Alford 2001). Winds also input power into the ocean to maintain the time-mean circulation and to generate subinertial fluctuations, either by the vertical or horizontal shear instability of the large-scale flows or directly via wind-induced

fluctuations at the ocean surface (Frankignoul and Müller 1979). The energy of both the subinertial fluctuations and the time-mean flow will be eventually dissipated (or transferred to the internal gravity wave field or small-scale turbulence). However, the exact portion of the power that escapes the turbulent mixed layer and that can potentially affect the interior mixing is still unknown.

In the oceanic interior, the near-inertial waves interact with the internal wave field and distribute their energy over a broad range of wavelengths and frequencies (Alford et al. 2016). At small wavelengths these waves are prone to vertical shear or gravitational instability and generate small-scale turbulence (or dissipate¹), which in turn effectively enhances molecular mixing of density. The near-inertial waves thus drive the large-scale motions via density changes that increase the potential energy of the ocean. The large-scale flows, in terms of

^a Current affiliation: Institute for Marine and Atmospheric Research, Utrecht University, Utrecht, Netherlands.

Corresponding author address: Antonija Rimac, Institute for Marine and Atmospheric Research, Utrecht University, Princetonplein 5, 3584 CC Utrecht, Netherlands.
E-mail: a.rimac@uu.nl

¹ Here, we use the word dissipation in a loose manner: Strictly, dissipation is the effect of molecular friction on kinetic energy. However, here we use the word in a more general sense as the transfer of total energy (e.g., gravity waves) to small-scale turbulence, or mesoscale eddies to gravity waves.

time means and variations at subinertial frequencies, can also generate density mixing that is similar to the dissipation of the internal gravity wave field (Tandon and Garrett 1996). Some of the processes that lead to the dissipation of the large-scale flows are bottom friction, lee-wave generation, topographic inviscid dissipation of a balanced flow, loss of balance resulting from the Lighthill radiation of gravity waves, gravity wave drag of the balanced flow, and direct generation of unbalanced ageostrophic instabilities (e.g., Molemaker et al. 2005; Dewar and Hogg 2010; Nikurashin and Ferrari 2011). Several of these processes will generate internal gravity waves or small-scale turbulence in the ocean's interior and thus could contribute to density mixing at different depths, which plays a key role in maintaining the ocean stratification and the meridional overturning circulation (Tandon and Garrett 1996; Melet et al. 2014).

In this study we focus on realistically quantifying the total energy flux to three different types of motions that is available for density mixing in the ocean interior. This energy flux includes both the vertical and the lateral fluxes that leave the ocean's spatially and seasonally varying mixed layer depth. The time-mean flow, and subinertial and near-inertial fluctuations are calculated from the same model output, but they are identified using a different time filter. Our estimate of the total energy flux provides an upper bound for the power available for the interior mixing, as the power input to subinertial fluctuations and the time-mean flow might generate mixing at a mixing efficiency lower than the power input to internal waves. Currently there is no realistic quantification of the total energy flux that includes the contributions from both different time scales and the spatially and seasonally varying mixed layer depth. We believe that the global estimate of this energy flux is important for understanding the general circulation and the energetics of the ocean.

Previous studies have focused on the amount of the wind-power input at the ocean surface, rather than the power input to the oceanic interior in the form of the energy flux leaving the surface mixed layer. Estimates of the total wind-power input to near-inertial motions at the sea surface range, depending on the observations and the chosen ocean models, between 0.3 and 1.1 TW (e.g., Alford 2001; Watanabe and Hibiya 2002; Alford 2003; Jiang et al. 2005; Furuichi et al. 2008; Simmons and Alford 2012; Jochum et al. 2013; Rimac et al. 2013). The wind-power input to the surface transient motions (including seasonal variations) ranges between 1.8 and 2.2 TW, and to the surface time-mean circulation between 1.85 and 2 TW (von Storch et al. 2007, 2012).

Some studies further assessed how much of the wind-power input to near-inertial motions at the surface is available for the ocean's interior. An assessment was conducted by considering vertical energy fluxes across a level at a constant depth. Using an ocean model at a $1/7^{\circ}$ horizontal resolution, Furuichi et al. (2008) estimated for different oceanic regions that approximately 75%–85% of the annual mean wind-power input to near-inertial motions is dissipated in the upper 150 m. Zhai et al. (2009) used a regional ocean model of the North Atlantic at a $1/12^{\circ}$ horizontal resolution and found that only 10% of the wind-power input to near-inertial motions from the ocean surface is transferred into the deep ocean below 230 m. Alford et al. (2012) examined the downward propagation of near-inertial wave energy following winter storms in the upper 800 m at Ocean Station Papa. They concluded that 12%–33% of the energy input transits 800 m toward the deep sea. Using a near-global 0.1° -resolution simulation, von Storch et al. (2007, their Table 2) found that of the total wind-power input at the ocean surface, 47% from the time-mean circulation and only 3% from the transient motions are passing through a 110-m-deep surface layer to the ocean beneath.

Several previous studies (e.g., Wunsch 1998; von Storch et al. 2007; Roquet et al. 2011), which focused on the wind-power input to the ocean's interior, were based on the theory of Stern (1975). This theory showed that the global integral of the product of the pressure and the Ekman pumping velocity at a level below the Ekman layer equals the global integral of the scalar product between the wind stress and the near-surface geostrophic velocity. However, this equality is satisfied only when applying the global area integral and assuming that the area to be integrated is at a geopotential surface. The energy fluxes based on the scalar product of wind stress and near-surface geostrophic velocity represent energy fluxes across, in Stern's words: "a constant level surface . . . that lies beneath the Ekman layer" (p. 114). Roquet et al. (2011) pointed out that these fluxes do not depend on the level used to calculate the surface geostrophic velocity. Although closely related, the energy flux obtained using Stern's equality differs from the flux across a spatially and seasonally varying mixed layer, which is the main aim of this study. We will also estimate the difference in the fluxes obtained using two different methods.

In the following section, we detail the model configuration that is used for the estimation of the surface energy input and the fluxes leaving the mixed layer, and we describe the method used to decompose the fluxes into near-inertial, subinertial, and time-mean components. In sections 3a and 3b, we present the results of the

wind-power input to the three components of motion at the sea surface and across the mixed layer, and we provide estimates of the fraction of the energy flux leaving the mixed layer. In section 3c, we discuss the role of Ekman dynamics for the wind-power input to the time-mean circulation and to the subinertial fluctuations. Then we address how our study relates to Stern's method and address the difference between estimates based on the mixed layer and those based on the Ekman layer (section 3d). In section 3e, we show that the local wind stress strength and mixed layer depth are the main factors controlling the fraction of the energy flux related to transient motions. A summary and discussions are given in the final section.

2. The ocean model and the data considered

We use an ocean-only simulation performed using the $1/10^{\circ}$ Max Planck Institute Ocean Model (MPI-OM; [von Storch et al. 2012](#)). The same model but at a lower horizontal and vertical resolution was used by [Rimac et al. \(2013\)](#). MPI-OM is a global ocean model based on the primitive equations, thus including the hydrostatic and Boussinesq approximations ([Olbers et al. 2012](#)). A primitive equation model can correctly simulate low-mode long internal waves that fall into the hydrostatic regime ([Gill 1982](#); [Simmons and Alford 2012](#)). The dominant meridional wavelengths of near-inertial waves obtained with this ocean model are 200–500 km, which compare well with the 200–600-km waves from [Simmons and Alford \(2012\)](#). The model is formulated on a tripolar grid with a grid size of approximately 10 km near the equator that decreases to 2.4 km toward the South Pole. The 80 vertical levels increase in thickness from 10 to 15 m in the surface layers to approximately 280 m at the bottom.

In MPI-OM, turbulent mixing and dissipation in the upper ocean are parameterized using a Richardson number-dependent mixing scheme ([Pacanowski and Philander 1981](#)). The resulting diffusion coefficient is augmented by an additional contribution describing the wind-induced mixing close to the ocean surface. This contribution takes the form of a cubic function of the local 10-m wind speed that decays exponentially with depth. It is dependent on the local static stability and is reduced in proportion to the fractional sea ice cover. The mixing scheme provides a realistic dissipation of near-inertial energy in the upper ocean and a realistic simulation of the mixed layer depth.

The model is spun up for 25 years using the German Ocean Model Intercomparison Project (OMIP) climatological forcing ([Röske 2006](#)), and ran for an additional 60 years using surface fluxes of heat and momentum

derived from the 6-hourly National Centers for Environmental Prediction (NCEP) reanalysis at approximately 1.875° resolution ([Kalnay et al. 1996](#)). The freshwater flux calculated from evaporation and precipitation is supplemented by daily river discharges at approximately 1.125° resolution.

For our analysis, daily data for the period 2001–06 and hourly data for January and July 2005 are used. The 6 years of daily data are used to quantify subinertial and time-mean motions and to estimate the 6-yr mean annual cycle of the mixed layer depth. The 2 months of hourly data are used to quantify near-inertial motions.

For each of the three forms of motions, we examine two quantities: 1) the work done by the winds at the sea surface in the form of the scalar product of wind stress and surface horizontal velocity, and 2) the energy flux leaving the mixed layer. The latter is calculated in two steps. First, to obtain the three-dimensional energy flux we calculate the product $p\mathbf{u}$ of the dynamically relevant pressure p , which was obtained by subtracting the reference hydrostatic pressure $gz\rho_o$, from the full pressure and the three-dimensional ocean velocity \mathbf{u} . Second, we calculate the energy flux, leaving a mixed layer with a spatially varying bottom $z = -h$ by projecting $p\mathbf{u}$ onto the unit vector \mathbf{n} that is normal to the bottom of the mixed layer h , and is shown below:

$$p\mathbf{u} \cdot \mathbf{n} = pu \frac{\partial h}{\partial x} + pv \frac{\partial h}{\partial y} + pw. \quad (1)$$

The first two terms on the right-hand side of the Eq. (1) are the projection of horizontal energy flux on the slope of the mixed layer (called the projection term), while the third term is the vertical energy flux. The mixed layer depth, h is calculated for each calendar month separately using the daily mean potential temperature and salinity. We first calculate the depth at which the daily density change relative to its surface value exceeds 0.125 kg m^{-3} . For each calendar month, h is then defined as the multiyear monthly maximum of these daily depths. The final energy fluxes leaving the mixed layer, no matter whether they are related to near-inertial, subinertial, or time-mean motions, are then obtained by projecting these (multiyear) monthly mean values of $p\mathbf{u}$ onto h in the respective month and then averaged over all available months (i.e., over 2 months for fluxes related to near-inertial motions, since only 2 months of hourly data are available, and over 12 months for the fluxes related to subinertial fluctuations and time-mean flow). In this way, we take the seasonal variation of the mixed layer depth into account.

The spatial structure and the seasonal change of the mixed layer depth is illustrated in [Fig. 1](#) for April and

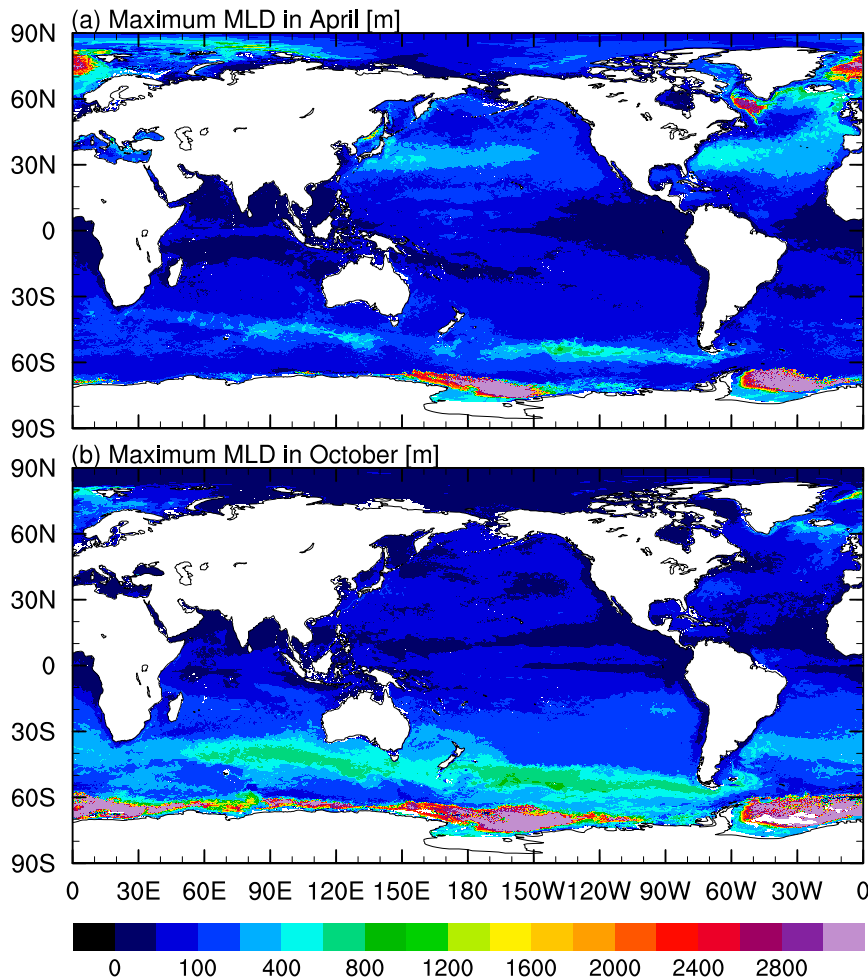


FIG. 1. Spatial distributions of the maximum mixed layer depth (MLD) for (a) April and (b) October diagnosed using the potential density criterion defined by [Levitus \(1982\)](#).

October, the two months when the mixed layer depth reaches its maximum, that is, up to a few hundred meters in the northern and southern mid- and high-latitude oceans. [Griffies et al. \(2009\)](#) showed that the mixed layer depth in several state-of-the-art numerical ocean models, including an earlier version of the MPI-OM, is overestimated at high latitudes. To evaluate the role of the overestimated mixed layer depth on our result, we repeat our calculation by excluding regions with mixed layer depth greater than 2000 m and find that the global energy fluxes vary less than 2%. Figure 1 also shows that the mixed layer depth deviates considerably from a surface at a constant depth. The difference between the shallowest depth of about a few tens of meters in the tropical oceans and the deepest depth of more than 1000 m in the high latitudes suggests a strongly inclined bottom of the mixed layer. An exact comparison of h with observations is not possible due to a very coarse temporal (monthly values) and spatial resolution of the

available observations. Nevertheless, the results shown in Fig. 1 are in broad agreement with the mixed layer depth derived from the Polar Science Center Hydrographic Climatology (PHC) data ([Steele et al. 2001](#)).

The total wind-power input and the total energy flux are approximately decomposed into the contribution from near-inertial motions $\overline{x^N y^N}$, the contribution from subinertial fluctuations $\overline{x' y'}$, and the contribution from the time-mean circulation $\overline{x} \overline{y}$ as follows:

$$\overline{x} \overline{y} \simeq \overline{x^N y^N} + \overline{x' y'} + \overline{x} \overline{y}. \quad (2)$$

For near-inertial motions we calculate an average over 2 months of hourly data, and for the subinertial fluctuations and the time-mean circulation we calculate an average over 6 years of daily data.

To obtain the power contribution from near-inertial motions, denoted by $\overline{x^N y^N}$ in Eq. (2), we integrate the cross-spectra between wind stress and surface horizontal

TABLE 1. Number of integer values used as an averaging period in a running-mean filter.

Latitude (°)	30	29–15	14–10	9–8	7–6	5	4
Period (day)	1	2	3	4	5	6	8

velocity, and between pressure and ocean three-dimensional velocity over the near-inertial frequency range ($0.7f < \omega < 1.3f$, where f denotes the local inertial frequency). These integrals of cross-spectra represent the covariances between two variables (wind stress and surface horizontal velocity or pressure and ocean velocity) at the near-inertial frequency range. We use the Daniell spectral estimator to estimate the cross-spectrum (von Storch and Zwiers 1999). The region of 4° latitude around the equator has been excluded from our analysis because of difficulties in estimating near-inertial energy in this region. The energy flux leaving the mixed layer is obtained by projecting $p^{\text{NI}} \mathbf{u}^{\text{NI}}$ in January and July onto the sloping bottom of the mixed layer in the respective month following Eq. (1), and then averaging over the values in these two months.

To obtain the power contribution from subinertial fluctuations, we use the daily anomalies obtained by subtracting, for each calendar month, the multiyear monthly means from the daily data. Using daily anomalies allows us to remove near-inertial signals poleward of 30° latitude, where inertial periods are shorter than one day. Equatorward of 30° , the daily data contain some near-inertial signals. To remove these signals, we apply different running-mean filters on the daily data equatorward of 30° latitude. The width of the running window, given in Table 1, is a function of latitude and equals the local inertial period rounded to the first higher integer number. The regions equatorward of 4° latitude will be excluded from the analysis, since the near-inertial period is longer than 7 days there, and hence it is not possible to separate it from the time scales of other transient motions. A daily variable that is low-pass filtered equatorward of 30° (using running windows defined in Table 1) is denoted by x' . The wind-power input is calculated from covariances $\tau' \cdot \mathbf{u}'_h$ between the low-pass-filtered daily anomalies of wind stress and surface horizontal velocity. The energy flux leaving the mixed layer is obtained by first calculating for each calendar month the covariances $\bar{p}' \mathbf{u}'$, and then projecting $\bar{p}' \mathbf{u}'$ onto the bottom of the mixed layer for the respective month. The overall subinertial energy flux leaving the mixed layer is obtained by averaging the projections over all calendar months.

To obtain the contribution from the time-mean motions, multiyear monthly means are used. The wind-power

input is calculated from the product of multiyear mean wind stress and multiyear mean surface horizontal velocity $\bar{\tau} \cdot \bar{\mathbf{u}}_h$. The energy flux leaving the mixed layer is obtained by first calculating for each calendar month the product $\bar{p} \bar{\mathbf{u}}$, where \bar{p} and $\bar{\mathbf{u}}$ are multiyear means for that month, and then projecting $\bar{p} \bar{\mathbf{u}}$ onto the bottom of the mixed layer in that month. The overall energy flux related to the time-mean flow is given as the average over fluxes in all calendar months. Note that the resulting fluxes include the seasonal cycle.

3. Results

a. Wind energy input at the sea surface

First, we estimate the wind-power input at the ocean surface to near-inertial motions ($\bar{\tau}^{\text{NI}} \cdot \mathbf{u}_h^{\text{NI}}$; Fig. 2a), the power input to subinertial fluctuations ($\bar{\tau}' \cdot \mathbf{u}'_h$; Fig. 2b), and the power input to the time-mean circulation ($\bar{\tau} \cdot \bar{\mathbf{u}}_h$; Fig. 2c). In the right panel we plot their respective zonal means. To smooth the noisy structure, here and in the following figures, all the fields are box averaged to a grid with a 0.4° resolution for better representation. All integrals are derived from the original output at $1/10^{\circ}$ resolution.

As in several previous studies (e.g., Rimac et al. 2013, and references therein), we find a large amount of the wind-power input to near-inertial motions (Fig. 2a) between 30° and 50°N and 20° and 50°S induced by midlatitude storms. The average energy input in the Northern Hemisphere is almost twice as large as in the Southern Hemisphere (with a hemispheric average of 1.1 mW m^{-2} in the Northern Hemisphere compared to 0.7 mW m^{-2} in the Southern Hemisphere). Conversely, the integrated energy input is slightly higher in the Southern Hemisphere (0.18 TW) compared to the Northern Hemisphere (0.17 TW) due to the larger coverage of the surface area in the Southern Ocean.

The energy input to subinertial fluctuations ($\bar{\tau}' \cdot \mathbf{u}'_h$; Fig. 2b) is positive almost everywhere. The highest values are found in the Southern Ocean, in the regions of the Kuroshio Extension and Gulf Stream, and in the subpolar gyre. The energy input to the time-mean circulation ($\bar{\tau} \cdot \bar{\mathbf{u}}_h$; Fig. 2c) is dominated by large values in the Southern Ocean. A larger energy input is seen between 40° and 60°S south of Africa and in the southern Indian Ocean, with a maximum value of about 0.2 W m^{-2} , than further east in the Pacific and in the Atlantic Ocean where the maximum is about 0.08 W m^{-2} . Large positive values in the time-mean circulation are also found in the Kuroshio Extension and Gulf Stream regions, while the tropical Pacific has zonal stripes of positive and negative values. In general, the energy input is largest to the

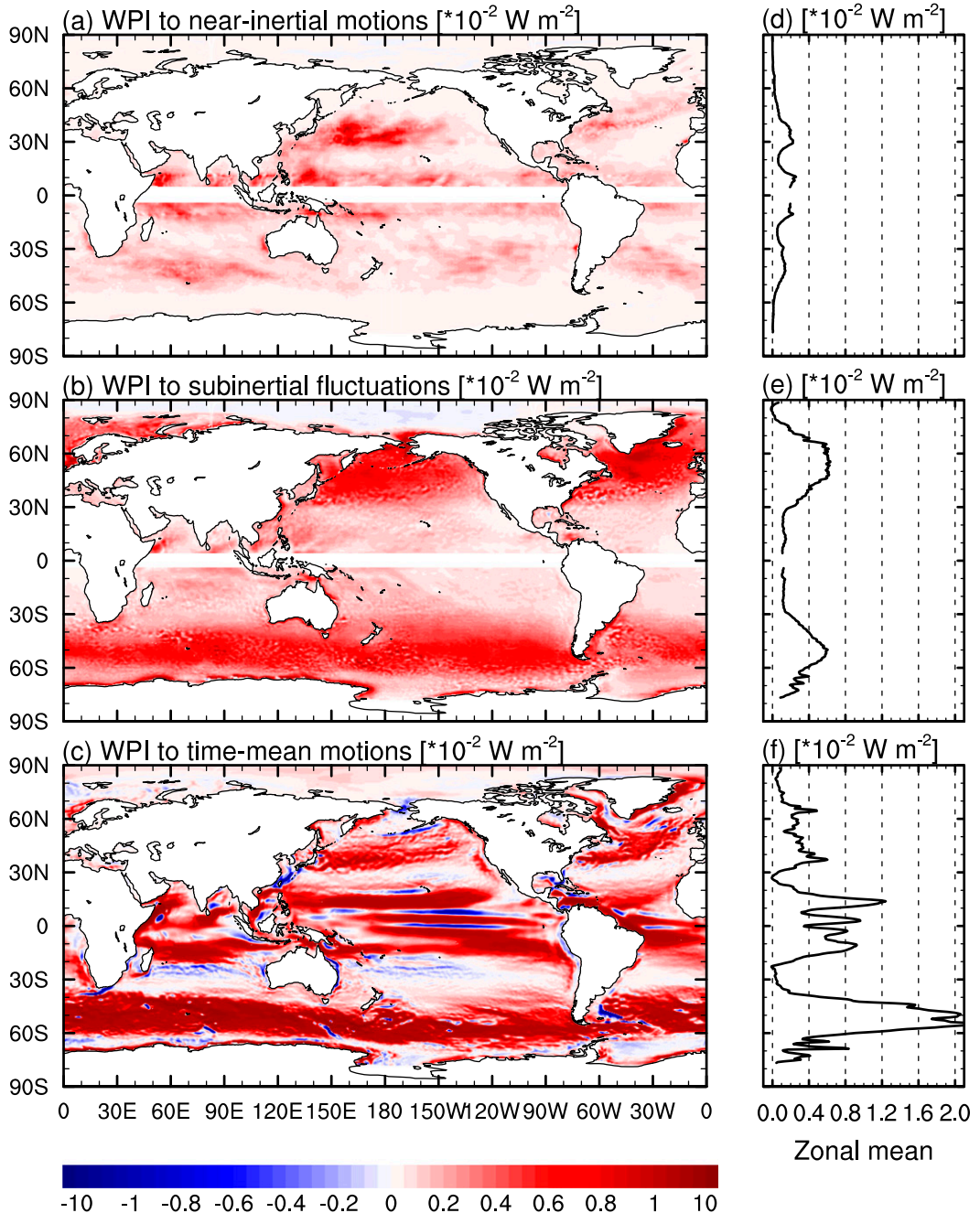


FIG. 2. Spatial distributions of the wind-power input (WPI) to (a) near-inertial motions, (b) subinertial fluctuations, and (c) time-mean circulation. (d)–(f) Zonal means for (a)–(c), respectively, are depicted. The color bar is highly nonlinear. Note the scaling factors on the top of each panel.

time-mean circulation, with highest values found in the Southern Ocean, and smallest to near-inertial motions. The largest energy input to subinertial fluctuations occurs in the midlatitude oceans.

The global integral of the wind-power input to near-inertial motions amounts to 0.35 TW (Table 2). This result compares well with results from previous studies.

For example, Furuichi et al. (2008) obtained a value of 0.4 TW using wind stress gridded at a 1.25° horizontal resolution and all four seasons of one year for their estimate. Simmons and Alford (2012) obtained a value of 0.36 TW using wind stress from the NCEP reanalysis. The global integral of the power input to subinertial fluctuations ($\overline{\tau' \cdot \mathbf{u}'_h}$) in our analysis amounts to 0.87 TW.

TABLE 2. Globally integrated wind-power input (INPUT), total energy flux leaving the mixed layer (FLUX), component due to the projection term in Eq. (1) (FLUX_p), the ratio of the integrated fluxes to the integrated energy input at the ocean surface (FRACTION), and the integrated fluxes from the projection term to the integrated energy input at the ocean surface (FRACTION $_p$). The plus and minus one standard deviations are used to quantify the robustness of the respective mean values.

	Near-inertial	Subinertial	Time-mean
INPUT (TW)	0.35	$0.87 \pm 4 \times 10^{-6}$	$2.11 \pm 3 \times 10^{-5}$
FLUX (TW)	0.04	$0.07 \pm 5 \times 10^{-4}$	0.81 ± 0.05
FRACTION (%)	11.4	8.04	38.4
FLUX_p (TW)	<0.01	<0.01	0.5
FRACTION $_p$ (%)	<1	<1	23.7

This number is lower than that provided by von Storch et al. (2007, 2012), partly because we consider only the subinertial fluctuations, rather than all transient motions, and partly because we exclude the equatorial regions. The global integral of the power input to the time-mean circulation ($\bar{\tau} \cdot \bar{\mathbf{u}}_h$) amounts to 2.11 TW. This number is in a broad agreement with those obtained by von Storch et al. (2007, 2012).

For the subinertial and time-mean contributions, we estimate the robustness of the global integrals by examining the effect of year-to-year variations on these integrals. This is done by calculating the standard deviation of the global integrals derived from each of the 6 years of wind-power inputs. The standard deviations (also listed in Table 2) suggest little variation over the considered years.

b. Energy flux leaving the ocean's mixed layer

The total energy flux leaving the mixed layer, together with its respective zonal means (black lines), is shown in Fig. 3, again for the three different types of motions. For the figures considered in this subsection, in addition to the box-average smoothing already introduced, we apply smoothing using running means with a radius of 100 km to smooth out very noisy structures in some regions.

The total near-inertial energy flux (Fig. 3a) is mainly positive, that is, leaving the mixed layer. Larger positive values are found in the midlatitude winter storm-track regions between 20° and 60°N and between 20° and 50°S. Positive values are also found in the tropical oceans. The global average of the total near-inertial energy flux leaving the mixed layer is 0.09 mW m^{-2} with a higher contribution in the Northern Hemisphere compared to the Southern Hemisphere.

The total energy flux to subinertial fluctuations (Fig. 3b) is mainly positive, that is, to the interior eddy field, in the regions of the subpolar gyres, the subtropical South Pacific, and the equatorial regions. The global average is 0.3 mW m^{-2} . The distribution reveals patchy structures concentrated in the Kuroshio Extension and Gulf Stream

regions, and in the Southern Ocean along the Antarctic Circumpolar Current (ACC).

The time-mean energy flux is more energetic than the energy fluxes from the subinertial and near-inertial fluctuations. The global average yields a downward flux of 5.6 mW m^{-2} , which is more than 15 times higher than the respective global average from subinertial fluctuations, and about 60 times higher than the global average of the near-inertial energy flux. The total time-mean energy flux is mainly positive but with patchy structures in the Southern Ocean between 40° and 70°S and in the Northern Hemisphere between 30° and 50°N. Large positive values are found off the equator in the subtropical regions.

To quantify the relative importance of the vertical flux pw and the projection term of the total flux $p\bar{u}\partial h/\partial x + p\bar{v}\partial h/\partial y$, both given in Eq. (1), we present the contributions from these two terms in Figs. 4 and 5, respectively. The total near-inertial energy flux is dominated by the downward vertical flux. The total subinertial energy flux is dominated by the positive vertical flux in the equatorial region, in the region of the subpolar gyre, and north and south of the ACC. The rest (i.e., the area along the ACC and in the Kuroshio Extension and Gulf Stream regions) results from a combination of the vertical flux and the projection term. The distribution of the projection term reveals many small-scale features of opposite signs. For the time-varying motions, the vertical flux is mainly positive and stronger than the horizontal flux. The time-mean flux is a combination of the vertical flux and the projection term. The two components have comparable strengths of opposite signs in the tropical oceans, in the Southern Ocean, and in the subpolar gyre region of the North Atlantic Ocean. The spatial scales of the vertical fluxes (Fig. 4c) are much larger than those of the projection term (Fig. 5c). The projection term is the strongest in the Southern Ocean between 40° and 70°S, in the regions of the Kuroshio Extension and Gulf Stream, and in the subpolar gyre region with varying positive and negative values. There is a tendency for the projection term to compensate for the vertical flux, which can be seen in the zonal mean plots (Fig. 4f vs Fig. 5f) in the tropical oceans,

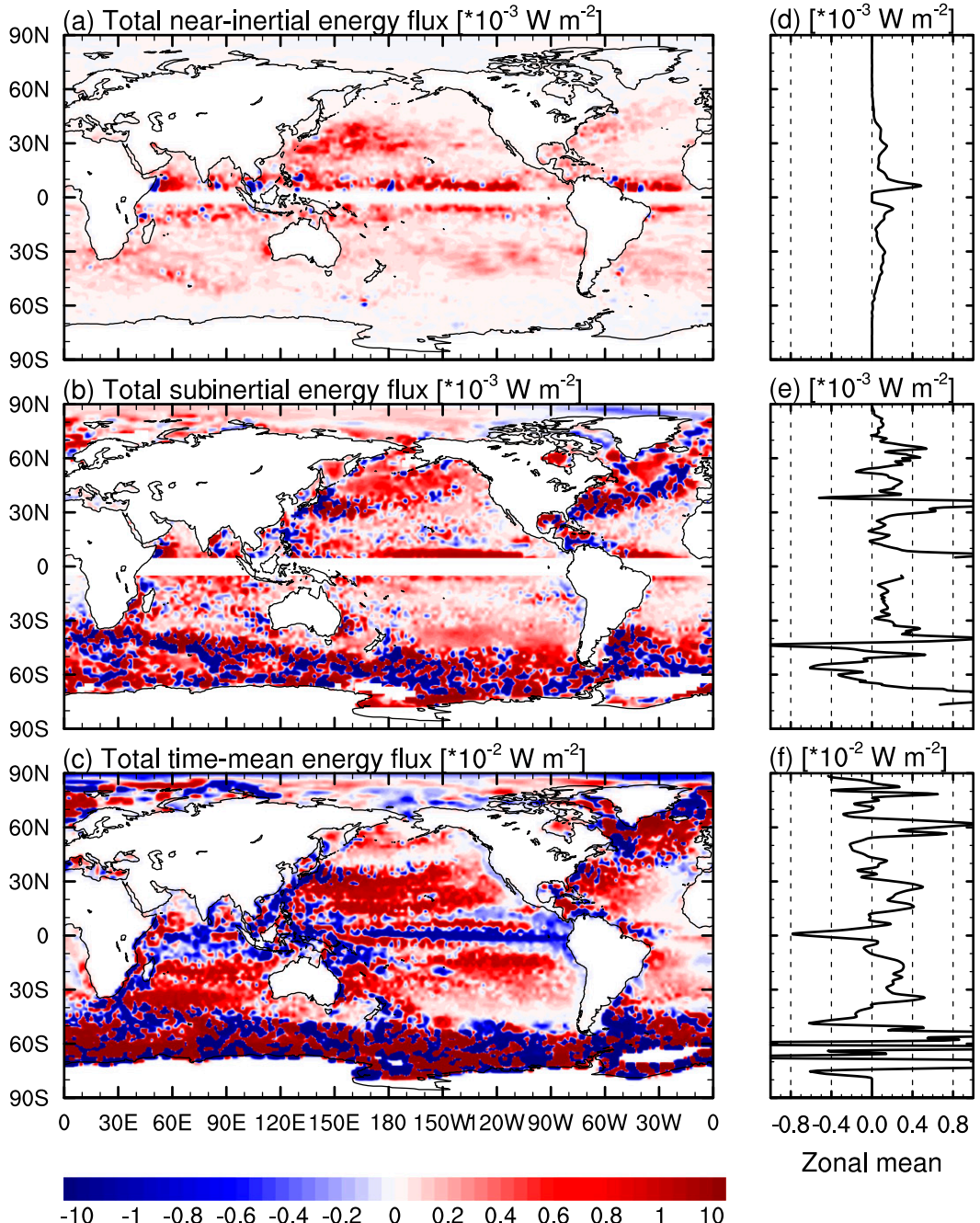


FIG. 3. Spatial distributions of (a) the total near-inertial energy flux, (b) the total energy flux from subinertial fluctuations, and (c) the total time-mean energy flux at the base of the mixed layer. (d)–(f) Zonal means for (a)–(c), respectively, are depicted. Note that positive values indicate downward energy fluxes. The color bar is highly nonlinear. Note the scaling factors on the top of each panel.

in the mid- and high-latitude Southern Ocean, and in the North Atlantic Ocean.

We calculate the global integrals of energy fluxes leaving the mixed layer (Table 2), and we estimate the fractions of the wind-power input at the sea surface that leave the mixed layer. For the near-inertial motions, the

global integral of the flux and its fraction are 0.04 TW and 11.4%, respectively. For subinertial fluctuations, the global integral of the energy flux and its fraction are 0.07 TW and 8.04%, respectively. For both the near-inertial and subinertial fluctuations, the projection term contributes less than 1% to the total energy flux. Therefore,

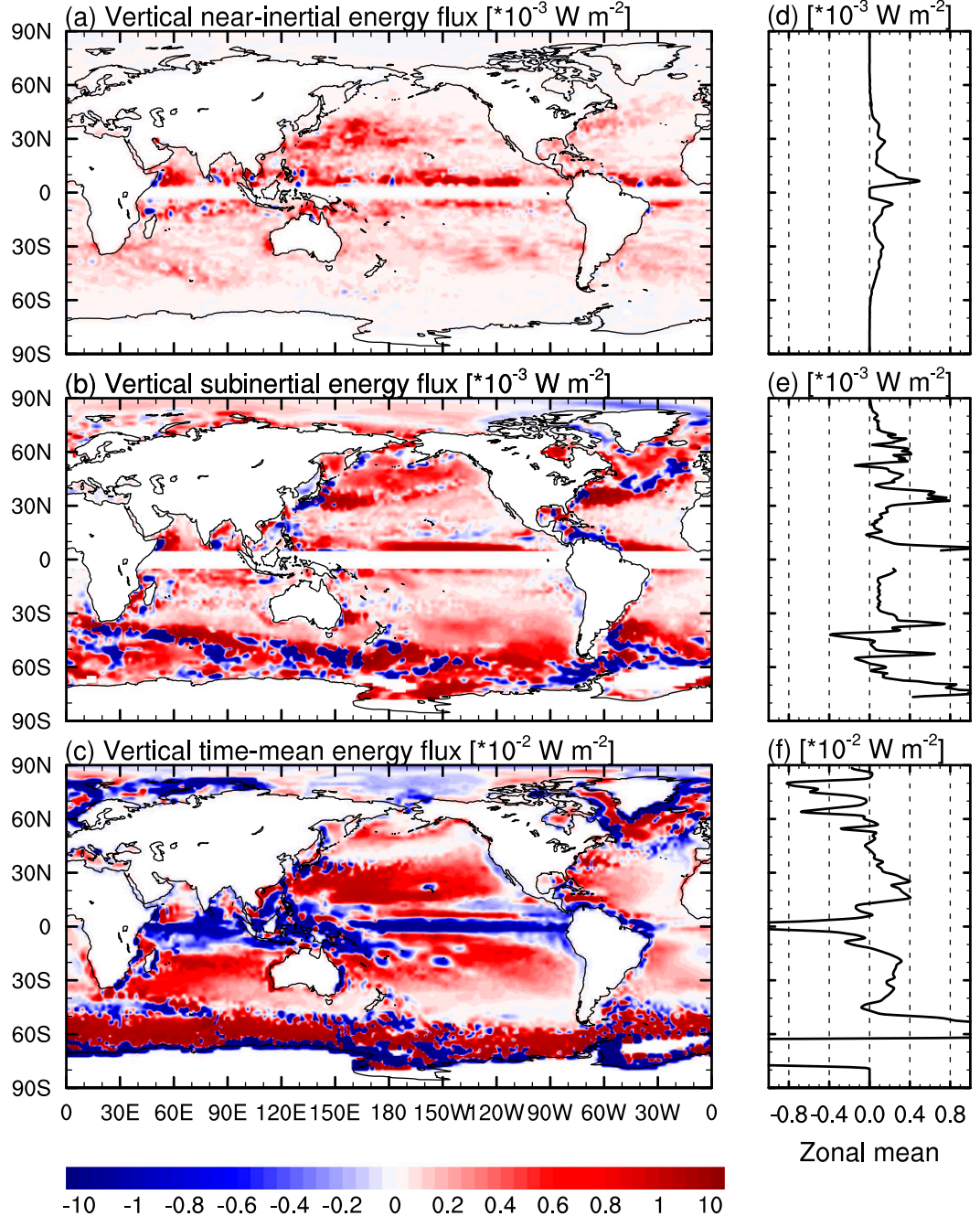


FIG. 4. Spatial distributions of (a) the vertical near-inertial energy flux, (b) the vertical energy flux from subinertial fluctuations, and (c) the vertical time-mean energy flux at the base of the mixed layer. (d)–(f) Zonal means for (a)–(c), respectively, are depicted. Note that positive values indicate downward energy fluxes. The color bar is highly nonlinear. Note the scaling factors on the top of each panel.

this term can be neglected and the knowledge about the vertical near-inertial and subinertial energy fluxes leaving the mixed layer is sufficient for estimating the power available for deep-ocean mixing.

For the time-mean motions, the global integral of the total energy flux leaving the mixed layer amounts to

0.81 TW, leading to a fraction of 38.4%. In contrast to the energy flux from the time-varying motions, the projection term of the horizontal time-mean energy flux of 0.5 TW is significantly larger than 0.31 TW from the vertical flux. This result supports the analysis of Roquet et al. (2011) that the energy is transported laterally in the

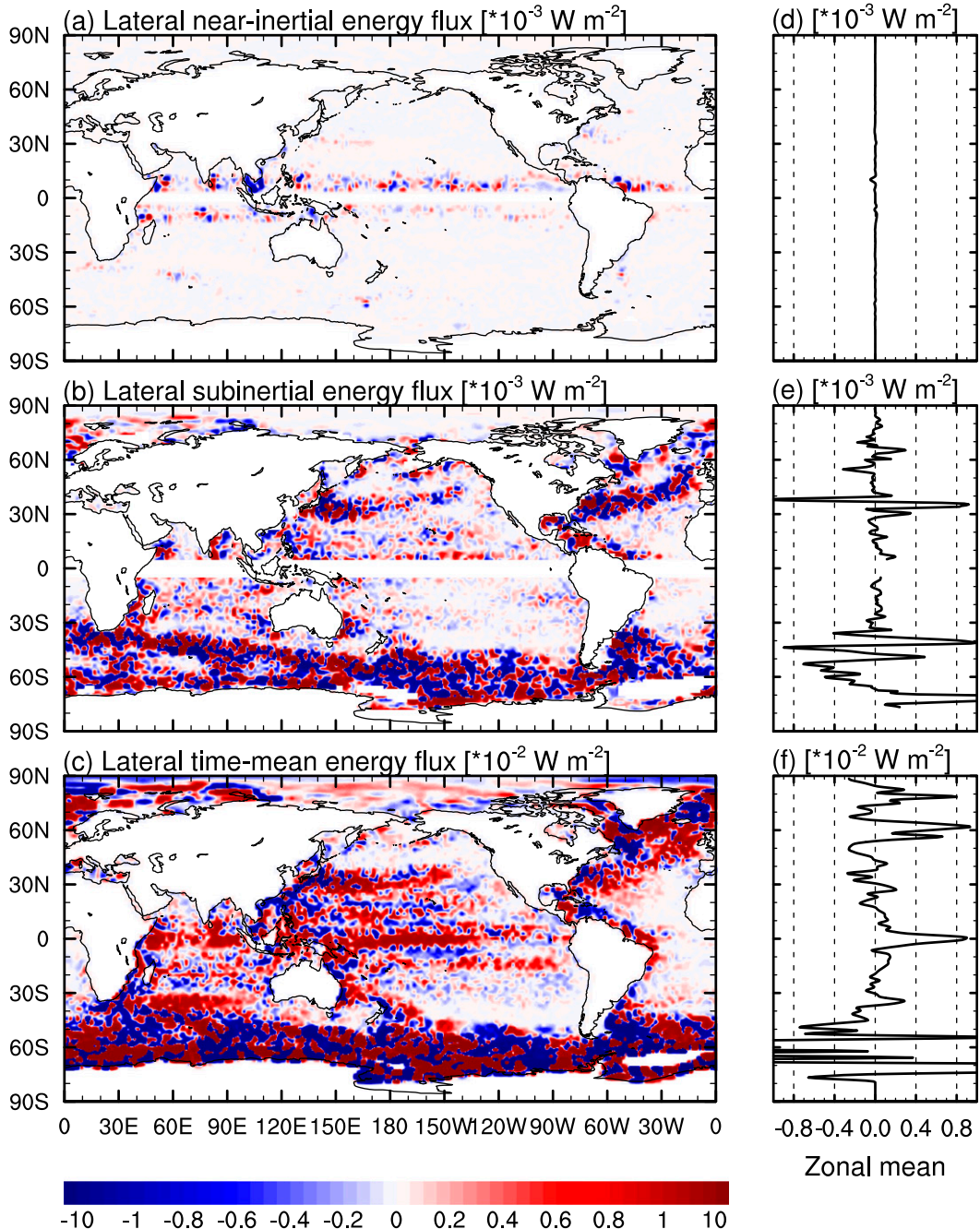


FIG. 5. Spatial distributions of the projection term of (a) the total near-inertial energy flux, (b) the projection term from the total energy flux from subinertial fluctuations, and (c) the projection term of the total time-mean energy flux at the base of the mixed layer. (d)–(f) Zonal means for (a)–(c), respectively, are depicted. Note that positive values indicate downward energy fluxes. The color bar is highly nonlinear. Note the scaling factors on the top of each panel.

Ekman layer and is consistent with the sloping bottom of the seasonally varying mixed layer. Overall, the energy flux leaving the mixed layer is largest for the time-mean motions, with a global integral approximately 12 times higher than the global integral from subinertial fluctuations

and more than 20 times higher than the global integral of the total energy flux from near-inertial waves.

We also calculate the standard deviations of transient and time-mean energy fluxes leaving the mixed layer to investigate the year-to-year variations of our

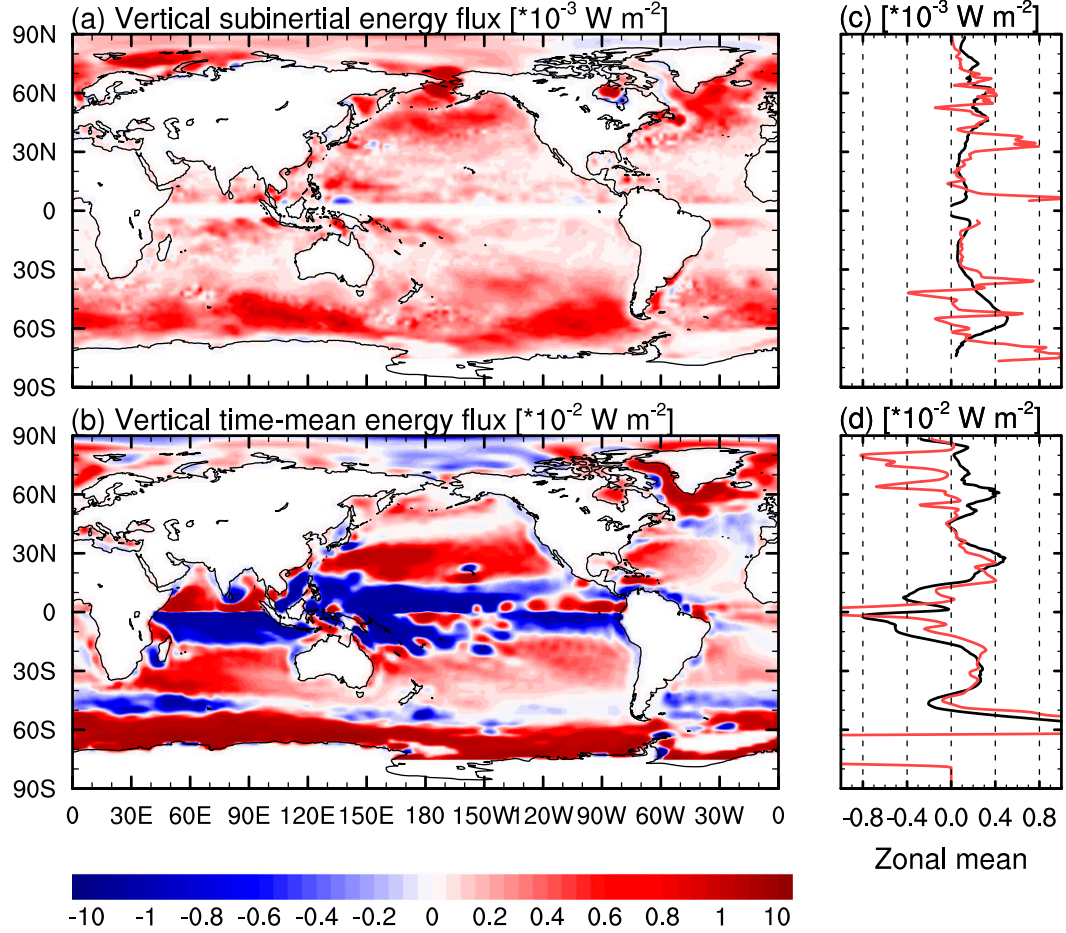


FIG. 6. (a),(b) As in Figs. 4b and 4c, except that the full vertical velocity is replaced with the Ekman velocity obtained from the wind stress curl. (c)–(d) Zonal means for (a)–(b), respectively, are depicted (black lines). For comparison, the respective zonal means from Figs. 4e and 4f are given in red. Positive values indicate downward energy fluxes. The color bar is highly nonlinear. Note the scaling factors on top of each panel.

global estimates. We conclude that these variations are weak.

c. Ekman dynamics as the dominant process for vertical energy flux

To understand the role of Ekman dynamics on the flux leaving the mixed layer, we calculate the vertical energy flux leaving the mixed layer. We replace the vertical velocity with the Ekman vertical velocity defined using the wind stress curl $w_E = \mathbf{k} \cdot \nabla \times \tau/f$, both for the flux related to subinertial fluctuations and that related to the time-mean flow. The two calculations, one using the vertical velocity and one using the Ekman vertical velocity, should be comparable if the Ekman dynamics are the main processes driving the vertical energy flux. In this case, a considerable part of the subinertial fluctuations would be externally forced by the winds, rather than originating from internal instability processes.

The large-scale structures of both $\overline{p'w'_E}$ and $\overline{p'w_E}$ in Figs. 6a and 6b roughly resemble those of $\overline{p'w'}$ and $\overline{p'w}$ in Figs. 4b and 4c. For the subinertial fluctuations, the largest differences are found in the ACC and in the Gulf Stream and Kuroshio Extension regions. Along the ACC, Fig. 4b shows patchy structures, whereas Fig. 6a shows positive values everywhere in the Southern Ocean. For the time-mean motions, the similarity between the pattern obtained from \overline{w} and that from $\overline{w_E}$ is somewhat stronger, in particular for the zonal mean profiles at low and midlatitudes (Fig. 6d). Large differences are found along the high-latitude coasts.

To further quantify the role of Ekman dynamics in transferring the wind power into subinertial fluctuations and time-mean motions, we calculate, at each grid point, the temporal correlations between the energy flux due to model vertical velocity w and that due to Ekman vertical velocity w_E (not shown). For subinertial fluctuations,

TABLE 3. Global integrals of the vertical energy fluxes across the mixed layer obtained using the model vertical velocity (row 1) and the vertical Ekman velocity (row 2), and those of the total energy fluxes across the mixed layer (row 3, taken from Table 2) and across the Ekman layer obtained by scalar multiplying the near-surface geostrophic velocity with the wind stress following Stern (1975) (row 4).

	Subinertial	Time-mean
FLUX _{ML,pw} (TW)	0.07	0.31
FLUX _{ML,pw_{Ekman}} (TW)	0.07	0.55
FLUX _{ML} (TW)	0.07	0.81
FLUX _{Stern} (TW)	0.13	1.32

daily data that are low-pass filtered equatorward of 30° latitudes are used. We found correlations higher than 80% in the North Atlantic and North Pacific subpolar gyres and in the subtropical to midlatitude South Pacific, where both Figs. 6a and 4b show downward fluxes. Correlations are low in the regions of the ACC, and in the Kuroshio Extension and Gulf Stream. The structure of the correlations suggests that the Ekman dynamics dominate only in regions with weak mesoscale eddies. In the ACC region, where large lateral density gradients are expected, the vertical energy flux leaving the mixed layer is dominated by the vertical velocities resulting from internal instabilities. The global mean correlation is approximately 45%, thus the effect of Ekman dynamics is considerable on average. For the time-mean motions, temporal correlations are calculated from long-term monthly mean data that reflect the mean annual cycle. Correlations higher than 80% are found in regions of both subtropical and subpolar gyres, indicating the dominant role of annual variations in Ekman pumping and sucking for the time-mean energy flux in those regions. The global mean correlation is approximately 48%.

For the subinertial fluctuations, the global integral of the vertical energy flux due to the Ekman vertical velocity $\bar{p}'\bar{w}'_E$, where p' is taken at the base of the mixed layer, is 0.07 TW (Table 3). This global integral is equal to that due to the model vertical velocity $\bar{p}'\bar{w}'$. For the time-mean motions, the global integral of the vertical energy flux due to the Ekman vertical velocity $\bar{p}\bar{w}_E$ is 0.55 TW, which is more than 40% higher than the value of 0.31 TW obtained with $\bar{p}\bar{w}$. This difference arises, mainly, from the differences along the northeast coast of North America, along the east coast of Greenland, and along the Antarctic coast.

d. Mixed layer versus Ekman layer

The energy flux derived from the three-dimensional velocity across a seasonally and spatially varying mixed layer differs considerably from the power injected into

the oceanic interior obtained by scalar multiplying wind stress with near-surface geostrophic velocity following Stern (1975; Table 3). The near-surface geostrophic velocities are derived from sea surface elevation as in Wunsch (1998). The subinertial and the time-mean motions are identified as described in section 2. The flux calculated following Stern (1975) is almost twice as large as the flux across the mixed layer (0.13 vs 0.07 TW) for the subinertial fluctuations and about 40% higher than the flux across the mixed layer (1.32 vs 0.81 TW) for the time-mean motions. The global integral of power to near-surface geostrophic motions $\tau \cdot \mathbf{u}_g$ equals the global integral of the energy flux across a geopotential surface beneath the Ekman layer (Stern 1975), although this equality is subjected to various approximations (von Storch et al. 2007). The values obtained using Stern's method are substantially larger than the energy fluxes leaving the mixed layer, suggesting that the Ekman layer is, on average, shallower than the mixed layer, at least in our model.

The global integrals of the energy fluxes across the Ekman layer following Stern (1975) were estimated using data derived from observations and a simulation using an alternative OGCM (Wunsch 1998; von Storch et al. 2007). In his study, Wunsch (1998) estimated the global integrals of the time-mean energy flux and of the flux to time-varying motions to be 0.84 and 0.04 TW, respectively. He used satellite altimeter data sampled every 10 days and the wind stress from the NCEP reanalysis averaged over the same 10-day period. von Storch et al. (2007) used the OFES model forced with daily wind stress from the NCEP reanalysis and estimated the time-mean energy flux of 0.92 TW and the flux to time-varying motions of 0.14 TW. The large time-mean value of 1.32 TW calculated in this study is likely related to the fact that the stand-alone MPI-OM overestimates the strength of the ACC and produces a Drake Passage transport of about 230 Sv ($1 \text{ Sv} \equiv 10^6 \text{ m}^3 \text{ s}^{-1}$). Note that this overestimation does not necessarily affect our conclusion concerning the relative depth of the mixed layer to that of the Ekman layer, since the fluxes across the mixed layer and Ekman layer are derived from the velocities simulated by the same model. Other factors, such as the different temporal resolutions of the used forcing fields and the different definitions of the separation between time-mean and subinertial fluctuations, can also contribute to the differences between our and the previously estimated numbers.

e. Factors controlling the fraction of the transient energy flux leaving the mixed layer

We identify two possible factors that might influence the fraction of the energy flux to time-varying motions

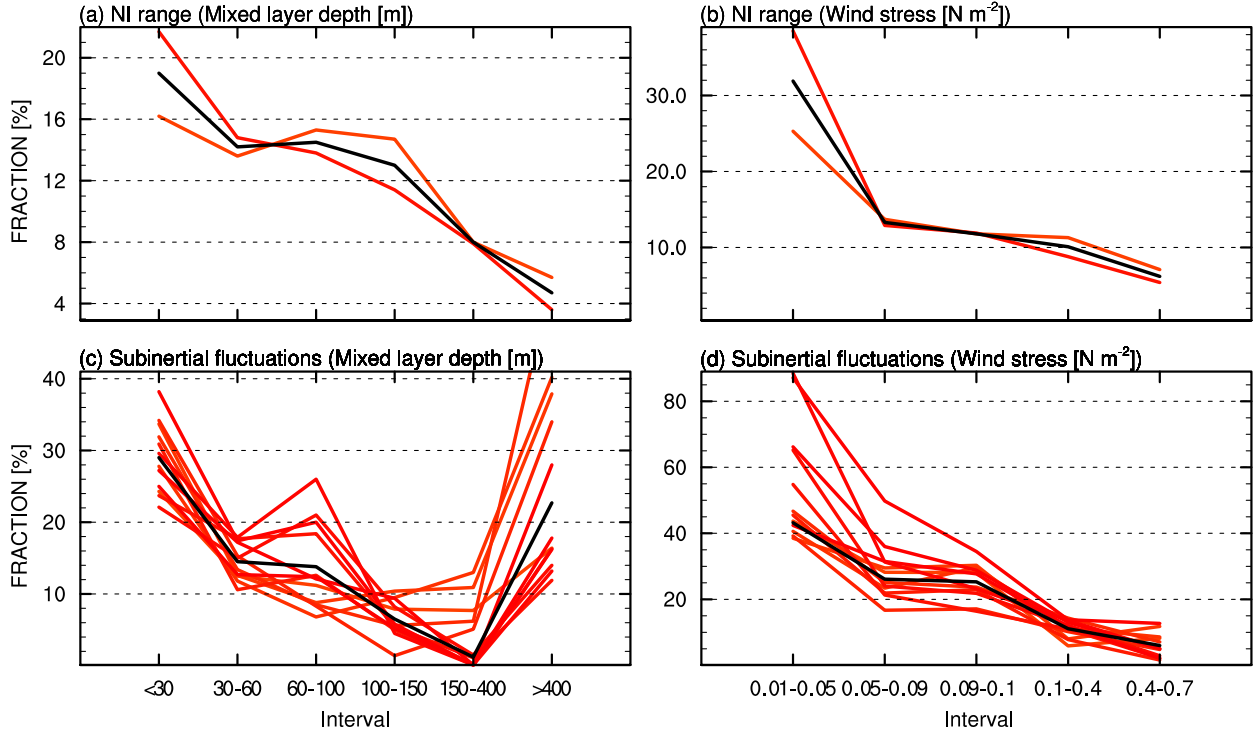


FIG. 7. Fractions of the (left) total energy flux as functions of mixed layer depth and (right) wind stress standard deviation for motions in the (a),(b) NI frequency range and (c),(d) for subinertial fluctuations. The red lines represent the contributions from each month, and the black lines are their means. Mixed layer depth and wind stress standard deviation are sorted and used to define the spatial domains for which we estimate the fractions. For example, <30 m in the mixed layer depth interval means that the fraction is calculated over all grid points where the mixed layer is less than 30 m deep.

that leaves the mixed layer. One factor is the wind stress variability. Obviously, stronger wind stress variability leads to a larger energy input to time-varying motions. However, stronger wind stress variability also implies a stronger mixing of momentum and thus stronger wind-induced dissipation within the mixed layer. In MPI-OM, the vertical momentum mixing is based on a Richardson number-dependent formulation that is augmented to take the near-surface wind stirring into account. Turbulent mixing in the ocean mixed layer is thus influenced by variability in the 10-m wind speed and by wind-induced changes in the vertical shear. For both processes, stronger wind stress variability leads to stronger dissipation inside the mixed layer and produces smaller values of the fraction. Thus, wind stress variability has two effects on the fraction, a productive role through increasing the energy input and a dissipative role through reducing the flux leaving the mixed layer.

Another factor affecting the magnitude of the fraction of energy flux leaving the mixed layer can be the mixed layer depth. A deeper mixed layer implies stronger dissipation because of the stronger shear at its base. As a consequence, the magnitude of the fraction should

decrease with increasing mixed layer depth. On the other hand, the mixed layer depth depends on the wind stress variability and the strong dissipation of wind-induced processes, which decrease the fraction as discussed above. Both factors, the wind stress variability and the mixed layer depth, are expected to play a role in the time-varying energy flux, not only on the near-inertial but also on subinertial time scales.

The effects of mixed layer depth and wind stress variability on the fraction of time-varying near-inertial and subinertial energy fluxes leaving the mixed layer are assessed by integrating the wind-power input and the energy fluxes, respectively, over areas with certain ranges of the mixed layer depth or the wind stress variability and calculating the fractions from these area integrals (Fig. 7). For near-inertial waves we define the wind stress variability as the time-mean standard deviation using NCEP wind data for January and July from 2005 separately. For subinertial fluctuations this variability is defined again as a standard deviation but using 6 years of daily mean wind stress for the respective month. The analyses for near-inertial waves are calculated for January and July (red lines), and the analyses

for subinertial fluctuations are calculated for each calendar month separately (red shading lines). For both near-inertial (NI) motions (Figs. 7a and 7b) and subinertial fluctuations (Figs. 7c and 7d), we find that the value of the fraction of the total energy flux decreases with increasing depth of the mixed layer. One exception seen in the fraction from subinertial fluctuations is the area with an extremely deep mixed layer (i.e., depth ≥ 400 m). Furthermore, the fraction decreases with the increasing strength of the wind stress variability. Our result supports the link between the mixed layer depth and the dissipation of time-varying motions inside the mixed layer. We could not find any connection of the time-mean flux to the wind stress variability or to the mixed layer depth.

4. Conclusions and discussion

In this study, we present an estimate of the fraction of the total energy flux that leaves the ocean's seasonally and spatially varying mixed layer. The estimate is derived for motions at the near-inertial, subinertial, and time-mean part of the energy spectrum, using the same output from a global ocean-alone $1/10^\circ$ simulation. Since daily fluctuations equatorward of 30° latitudes are influenced by near-inertial signals, we apply a running-mean filter on daily data to remove these signals. We conclude the following:

- From 0.35 TW of the wind-power input to near-inertial motions, only 0.04 TW, or 11.4%, leaves the mixed layer. From 0.87 TW of the wind input to subinertial fluctuations, 0.07 TW, or 8.04%, leaves the mixed layer. From 2.11 TW of the time-mean (including the seasonal cycle) wind input, 0.81 TW, or 38.4%, leaves the mixed layer. The total wind-power input amounts to 3.33 TW. Of that, 72.3% is dissipated (or converted into some other form of energy) within the mixed layer and 0.92 TW is radiated across the mixed layer into the ocean interior.
- For the transient motions, the total energy flux leaving the mixed layer results mainly from the vertical fluxes. For the time-mean flow, only 40% of the total flux results from vertical fluxes and the other 60% results from the projection of horizontal fluxes onto the sloping mixed layer.
- The spatial structure of the vertical flux leaving the mixed layer is closely related to the Ekman velocity and hence to the wind stress curl. For the subinertial fluctuations, the global integral of the energy flux across the mixed layer due to the full vertical velocity is identical to that due to the vertical Ekman velocity, despite local differences. For the time-mean motions, the global integral of the flux caused by the Ekman velocity is higher than that obtained using the full velocity.

- The globally integrated total flux across the seasonally and spatially varying mixed layer is approximately 40%–50% weaker than the flux calculated using the wind stress and the surface geostrophic velocity, suggesting that the mixed layer extends below the Ekman layer.
- A deeper mixed layer and a stronger wind stress forcing imply a stronger net dissipation of time-varying motions and hence smaller values of the fraction. The wind stress forcing generates time-varying motions but also dampens these motions via enhanced turbulent mixing inside the mixed layer. These dependencies can be implemented in energy-based mixing closures but need further consideration.

We found considerable wind-induced flux to subinertial fluctuations, predominantly related to mesoscale eddies, with an average for the midlatitude oceans of 3 mW m^{-2} . This seems surprising since it is expected that baroclinic and barotropic instabilities of the mean flow, rather than the wind forcing, are the sources of eddy energy in the ocean. Using a realistic broadband wind stress spectrum and integrating the effect of the wind forcing on the oceanic quasigeostrophic eddies, [Frankignoul and Müller \(1979\)](#) estimated an energy input rate of the order of 1 mW m^{-2} in the midlatitudes. Our estimate is even larger and shows up in regions where the sources of eddy energy due to instabilities are weak and the Ekman dynamics dominate. This result thus points toward the importance of wind forcing in generating subinertial fluctuations, which might need consideration in eddy closures.

It has been shown (e.g., [Duhaut and Straub 2006](#); [Zhai et al. 2012](#)) that when the relative motions between the ocean and the atmosphere are accounted for in the wind stress calculation, the wind stress mechanically damps the mesoscale eddies by reducing the wind input up to 70%. [Duhaut and Straub \(2006\)](#) suggested that to some extent the observed ocean velocity should be replaced by the actual model surface velocity in the wind stress calculation to compensate for this reduction. [Rath et al. \(2013\)](#) further found that accounting for the ocean surface velocity dependence in the surface momentum flux leads to a reduction of the wind-power input to near-inertial motions and a reduction of near-inertial energy in the mixed layer by approximately 20%. Since in our model we do not account for this dependence of the wind stress on ocean velocity, the energy fluxes estimated here likely have a bias of the same 20%, as estimated by [Rath et al. \(2013\)](#). However, we do not expect this bias to affect the respective fraction of the fluxes leaving the mixed layer, since a smaller input would also lead to a smaller flux leaving the mixed layer.

The amount of energy being transferred to the deep ocean has been studied following Stern's consideration (e.g., Wunsch 1998; von Storch et al. 2007; Roquet et al. 2011). Here, we concentrate on the energy flux leaving the mixed layer, since this is the effective flux that "survives" the mixed-layer dissipation and becomes available to be "received" by the interior ocean. We found that this flux is approximately 40%–50% weaker than the flux obtained following Stern's consideration. The latter should be interpreted as a flux across the Ekman layer. The discrepancy results partly from the fact that the Ekman layer is shallower than the mixed layer and partly from the projection of strong lateral fluxes across the sloped bottom of the mixed layer, which tend to compensate the mostly downward-orientated vertical fluxes.

The present results, in particular the part regarding the factors controlling the fraction of the flux leaving the mixed layer to the total wind input, are closely linked to the mixing parameterization implemented in the MPI-OM. Further studies are required to investigate how strongly our results depend on the used mixing parameterizations.

Acknowledgments. Numerical computations were performed, and the data used for the analyses are archived at the German Climate Computer Center (DKRZ). We thank Helmuth Haak for his input. We also thank two reviewers for their comments on a previous version of this manuscript.

REFERENCES

- Alford, M., 2001: Internal swell generation: The spatial distribution of energy flux from the wind to mixed layer near-inertial motions. *J. Phys. Oceanogr.*, **31**, 2359–2368, doi:10.1175/1520-0485(2001)031<2359:ISGTS>2.0.CO;2.
- , 2003: Improved global maps and 54-year history of wind-work on ocean inertial motions. *Geophys. Res. Lett.*, **30**, 1424, doi:10.1029/2002GL016614.
- , M. Cronin, and J. Klymak, 2012: Annual cycle and depth penetration of wind-generated near-inertial internal waves at Ocean Station Papa in the northeast Pacific. *J. Phys. Oceanogr.*, **42**, 889–909, doi:10.1175/JPO-D-11-092.1.
- , J. MacKinnon, H. Simmons, and J. Nash, 2016: Near-inertial internal gravity waves in the ocean. *Annu. Rev. Mar. Sci.*, **8**, 95–123, doi:10.1146/annurev-marine-010814-015746.
- Dewar, W., and A. Hogg, 2010: Topographic inviscid dissipation of balanced flow. *Ocean Modell.*, **32**, 1–13, doi:10.1016/j.ocemod.2009.03.007.
- Duhaut, T., and D. Straub, 2006: Wind stress dependence on the ocean surface velocity: Implications for mechanical energy input for ocean circulation. *J. Phys. Oceanogr.*, **36**, 202–211, doi:10.1175/JPO2842.1.
- Frankignoul, C., and P. Müller, 1979: Quasi-geostrophic response of an infinite β -plane ocean to stochastic forcing by the atmosphere. *J. Phys. Oceanogr.*, **9**, 104–127, doi:10.1175/1520-0485(1979)009<0104:QGOA>2.0.CO;2.
- Furuichi, N., T. Hibiya, and Y. Niwa, 2008: Model-predicted distribution of wind-induced internal wave energy in the world's oceans. *J. Geophys. Res.*, **113**, 768, doi:10.1029/2008JC004768.
- Gill, A., 1982: *Atmosphere-Ocean Dynamics*. Academic Press, 662 pp.
- Griffies, S., and Coauthors, 2009: Coordinated Ocean-ice Reference Experiments (CORES). *Ocean Modell.*, **26**, 1–46, doi:10.1016/j.ocemod.2008.08.007.
- Jiang, J., Y. Lu, and W. Perrie, 2005: Estimating the energy flux from the wind to ocean inertial motions: The sensitivity to surface wind fields. *Geophys. Res. Lett.*, **32**, L15610, doi:10.1029/2005GL023289.
- Jochum, M., B. Briegleb, G. Danabasoglu, W. Large, N. Norton, S. Jayne, M. Alford, and F. Bryan, 2013: On the impact of oceanic near-inertial waves on climate. *J. Climate*, **26**, 2833–2844, doi:10.1175/JCLI-D-12-00181.1.
- Kalnay, E., and Coauthors, 1996: The NCEP/NCAR 40-Year Reanalysis Project. *Bull. Amer. Meteor. Soc.*, **77**, 437–471, doi:10.1175/1520-0477(1996)077<0437:TNYRP>2.0.CO;2.
- Levitus, S., 1982: Climatological atlas of the world ocean. NOAA Professional Paper 13, 173 pp.
- Melet, A., R. Hallberg, A. Legg, and M. Nikurashin, 2014: Sensitivity of the ocean state to lee wave–driven mixing. *J. Phys. Oceanogr.*, **44**, 900–921, doi:10.1175/JPO-D-13-072.1.
- Molemaker, M., J. McWilliams, and I. Yavneh, 2005: Baroclinic instability and loss of balance. *J. Phys. Oceanogr.*, **35**, 1501–1517, doi:10.1175/JPO2770.1.
- Munk, W., and C. Wunsch, 1998: Abyssal recipes II: Energetics of tidal and wind mixing. *Deep-Sea Res. I*, **45**, 1977–2010, doi:10.1016/S0967-0637(98)00070-3.
- Nikurashin, M., and R. Ferrari, 2011: Global energy conversion rate from geostrophic flows into internal lee waves in the deep ocean. *Geophys. Res. Lett.*, **38**, L08610, doi:10.1029/2011GL046576.
- Olbers, D., J. Willebrand, and C. Eden, 2012: *Ocean Dynamics*. Springer, 704 pp., doi:10.1007/978-3-642-23450-7.
- Pacanowski, R., and S. Philander, 1981: Parametrization of vertical mixing in numerical models of tropical oceans. *J. Phys. Oceanogr.*, **11**, 1443–1451, doi:10.1175/1520-0485(1981)011<1443:POVMIN>2.0.CO;2.
- Rath, W., R. Greatbatch, and X. Zhai, 2013: Reduction of near-inertial energy through the dependence of wind stress on the ocean-surface velocity. *J. Geophys. Res. Oceans*, **118**, 2761–2773, doi:10.1002/jgrc.20198.
- Rimac, A., J.-S. von Storch, C. Eden, and H. Haak, 2013: The influence of high-resolution wind stress field on the power input to near-inertial motions in the ocean. *Geophys. Res. Lett.*, **40**, 4882–4886, doi:10.1002/grl.50929.
- Roquet, F., C. Wunsch, and G. Madec, 2011: On the patterns of wind-power input to the ocean circulation. *J. Phys. Oceanogr.*, **41**, 2328–2342, doi:10.1175/JPO-D-11-024.1.
- Röske, F., 2006: A global heat and freshwater forcing dataset for ocean models. *Ocean Modell.*, **11**, 235–297, doi:10.1016/j.ocemod.2004.12.005.
- Simmons, H., and M. Alford, 2012: Simulating the long-range swell of internal waves generated by ocean storms. *Oceanography*, **25**, 30–41, doi:10.5670/oceanog.2012.39.
- Steele, M., M. Morley, and W. Ermold, 2001: PHC: A global ocean hydrography with a high-quality Arctic Ocean. *J. Climate*, **14**, 2079–2087, doi:10.1175/1520-0442(2001)014<2079:PAGOHW>2.0.CO;2.
- Stern, M., 1975: *Ocean Circulation Physics*. Academic Press, 246 pp.

- Tandon, A., and C. Garrett, 1996: On a recent parametrization of mesoscale eddies. *J. Phys. Oceanogr.*, **26**, 406–411, doi:[10.1175/1520-0485\(1996\)026<0406:OARPOM>2.0.CO;2](https://doi.org/10.1175/1520-0485(1996)026<0406:OARPOM>2.0.CO;2).
- von Storch, H., and F. Zwiers, 1999: *Statistical Analysis in Climate Research*. Cambridge University Press, 484 pp.
- von Storch, J.-S., H. Sasaki, and J. Marotzke, 2007: Wind-generated power input to the deep ocean: An estimate using a 1/10° general circulation model. *J. Phys. Oceanogr.*, **37**, 657–672, doi:[10.1175/JPO3001.1](https://doi.org/10.1175/JPO3001.1).
- , C. Eden, I. Fast, H. Haak, D. Hernandez-Deckers, E. Maier-Reimer, J. Marotzke, and D. Stammer, 2012: An estimate of the Lorenz energy cycle for the World Ocean based on the 1/10° STORM/NCEP simulation. *J. Phys. Oceanogr.*, **42**, 2185–2205, doi:[10.1175/JPO-D-12-079.1](https://doi.org/10.1175/JPO-D-12-079.1).
- Watanabe, M., and T. Hibiya, 2002: Global estimates of the wind-induced energy flux to inertial motions in the surface mixed layer. *Geophys. Res. Lett.*, **29**, 1239, doi:[10.1029/2001GL014422](https://doi.org/10.1029/2001GL014422).
- Wunsch, C., 1998: The work done by the wind on the oceanic general circulation. *J. Phys. Oceanogr.*, **28**, 2332–2340, doi:[10.1175/1520-0485\(1998\)028<2332:TWDBTW>2.0.CO;2](https://doi.org/10.1175/1520-0485(1998)028<2332:TWDBTW>2.0.CO;2).
- Zhai, X., R. Greatbatch, C. Eden, and T. Hibiya, 2009: On the loss of wind-induced near-inertial energy to turbulent mixing in the upper ocean. *J. Phys. Oceanogr.*, **39**, 3040–3045, doi:[10.1175/2009JPO4259.1](https://doi.org/10.1175/2009JPO4259.1).
- , H. Johnson, D. Marshall, and C. Wunsch, 2012: On the power input to the ocean general circulation. *J. Phys. Oceanogr.*, **42**, 1357–1365, doi:[10.1175/JPO-D-12-09.1](https://doi.org/10.1175/JPO-D-12-09.1).